ULTRA-HIGH GRADIENT ACCELERATION IN NANO-CRYSTAL CHANNELS*

Young-Min Shin†, Department of Physics, Northern Illinois University, Dekalb, IL 60115 and Accelerator Physics Center (APC), FNAL, Batavia, IL 60510, USA
Alex Lumpkin, Randy Michael Thurman-Keup, Vladimir Shiltsev, FNAL, Batavia, IL 60510, USA
Xiaomei Zhang, Shanghai Institute of Optics and Fine Mechanics, Shanghai, China
Deano Michael-Angelo Farinella, Peter Taborek, Toshiki Tajima, University of California - Irvine, Irvine, CA 92697, USA

Abstract

Excitation of plasma waves by short intense laser pulses or particle bunches results in very high accelerating gradients [1]. Crystals have ultimately high density of mobile charge carriers (electrons) ~ 10^{19} - 10^{23} cm^{-3} and therefore, under short intense EM impact, can possibly support electric fields of up to 30 TV/m of plasma oscillation [2 – 4]. Atomic lattice in solid crystals remains practically immobile during short impact pulse and its own focusing field of ~10 - 100 V/Å is capable of guiding and collimating high energy particles, thus, opening the way to continuously focused acceleration of heavy leptons (muons) to unprecedented energies [5]. Compared to natural crystal, nanostructured crystals, e.g. carbon nanotubes, with dimensional flexibilities can offer a few orders of magnitude larger phase-space volume for channelling particles [6, 7]. Here we present PIC simulation results obtained with two plasma acceleration codes, Vsim and EPOCH, indicating that in the linear regime the beam-driven or laser-driven channelling acceleration in a 100 μm long nanotube can impart to electrons a gain of up to 10 MeV of energy (G = 100 GeV/m). Experimental tests, including a slit-mask beam modulation and pump-probe electron diffraction, are being planned and prepared at Fermilab and NIU to demonstrate the wakefield acceleration in a photo-excited nano-crystal.

INTRODUCTION

Traveling wake fields in an ionized plasma media, excited by a short bunch of relativistic particles or by short pulse lasers promise extremely high acceleration gradients of G (max. gradient) = $m_e c\omega_p/e \approx 96 \times n_0^{1/2}$ [V/m], where $\omega_p = (4\pi n_p e^2/m_e)^{1/2}$ is the electron plasma frequency and n_p is the ambient plasma density [cm^{-3}], m_e and e are the electron mass and charge, respectively, and c is the speed of light in vacuum [1]. However, a practically obtainable plasma density (n_p) in ionized gas is limited to below ~ 10^{18} cm^{-3}, which in principle corresponds to wakefields up to ~ 100 GV/m, and it is realistically difficult to create a stable gas plasma with a charge density beyond this limit. Upon high frequency irradiation, metallic crystals can be considered as the naturally existing dense plasma media completely full with a large number of conduction electrons available for the wakefield interactions. The density of charge carriers (conduction electrons) in solids n_0 = ~ 10^{20} – 10^{23} cm^{-3} is significantly higher than what was considered above in gaseous plasma, and correspondingly the wakefield strength of conduction electrons in solids, if excited, can possibly reach O(10) TV/m in principle.

Carbon nanostructures have some advantages over the crystals for channeling applications of high power beams. The de-channeling rate can be reduced and the beam acceptance increased by the large size of the channels. For beam driven acceleration, a bunch length with a sufficient charge density would need to be in the range of the plasma wavelength to properly excite plasma wakefields, and channeled particle acceleration with the wakefields must occur before the ions in the lattices move beyond the restoring threshold. In the case of the excitation by short laser pulses, the dephasing length is appreciably increased with the larger channel, which enables channeled particles to gain a sufficient amount of energy. This paper describes simulation analyses on beam- and laser (X-ray)-driven accelerations in effective CNT models obtained from Vsim [8] and EPOCH [9] codes. Experimental setups to detect wakefields are also outlined with an accelerator facility in Fermilab and NIU.

SIMULATION DATA

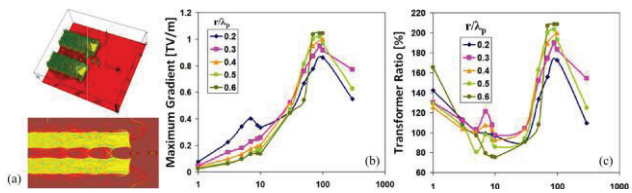

Figure 1: (a) Charge distribution of a nanotube acceleration ($n_p = n_b$) with a drive and witness beam (b) maximum acceleration gradient and (c) transformer ratio versus bunch charge distribution normalized by bunch charge density with various tunnel radii (r = 0.2 – 0.6λ_p).

Figure 1(a) shows a snapshot of a two-beam accelerating system with a ~10λ_p hollow plasma channel that is modeled with n_p ~ $10^{19}cm^{-3}$. The simulation condition also includes the drive-witness coupling distance of ~1.6λ_p, σ = ~ 0.1λ_p and a linear regime bunch charge density of n_b ~ n_p. For this simulation, the plasma channel is designed with a tunnel of r = 0.1λ_p. Just like a uniformly filled one, the drive bunch generates tailing

*Work supported by the DOE contract No.DEAC02-07CH11359 to the Fermi Research Alliance LLC.

ISBN 978-3-95450-147-2

wakes in the hollow channel due to the repulsive space charge force. The plasma waves travel along the hollow channel with the density modulation in the same velocity with the witness beam. Note that the bunch shape of the drive beam in the tunnel remains relatively longer than in the cylindrical plasma column. The energy versus distance plots in Fig. 1 shows that sinusoidal energy modulation apparently occurs in the plasma channel perturbed by two bunches. Here, the relative position of the drive beam corresponds to the first maximum energy loss, while that of the witness beam does to the first maximum energy gain. The traveling wakes around the tunnel continuously transform acceleration energy from the drive beam to the witness one. The energy gain and acceleration gradient are fairly limited by the radius and length of the tunnel with respect to plasma wavelength and bunch charge density. Bunch parameters of the beam-driven acceleration system have thus been analyzed with various tunnel radii, as shown in Fig. 1(b). For the analysis, the bunch charge density was swept from 1 to 300, normalized by plasma density, n_p, for five different tunnel radii from 0.2 to 0.6 λ_p and relativistic beam energy 20 MeV. While in the linear regime n_b = ~ 1 – $10n_p$, the maximum acceleration gradient drops off with an increase of the tunnel radius from 0.2 to 0.6, it increases in the blowout regime, n_b = ~ 10 – $100n_p$. The maximum acceleration gradient is increased from ~ 0.82 TeV/m of r = 0.2 λ_p to ~ 1.02 TeV/m of r = 0.6 λ_p with n_b = $100n_p$, corresponding to ~ 20% improvement. The energy transformer ratio follows a similar tendency with the acceleration gradient curve in the linear and blowout regimes. In the linear regime (n_b/n_p ~ 1 – 10), scattering is negligibly small, which does not perturb particle distribution of the bunch within the hollow channel. The repulsive space charge force between the bunch and the plasma is increased inversely proportional to their spacing. The channeled bunch thus undergoes higher acceleration gradient as the channel gets smaller, as shown in Fig. 1. However, in the blowout regime (n_b/n_p ~ 10 – 100), the repulsive space charge force from an excessive amount of the bunch charge density against the plasma channel is strong as to heavily perturb the bunch and to scatter electrons out of the bunch. The strength of space charge force is decreased with the channel radius, so the electrons in the bunch is less scattered with an increase of the channel radius. The gradient is thus lowered with an increase of the channel radius accordingly. The similar tendency also appears on the transformer ratio, as shown in Fig. 1(c). The energy is more efficiently converted from the drive beam to the witness one with the larger channel in the blowout regime, although the transformer ratio does not similarly follow the tendency of accelerating gradient with the channel size in the linear regime. The un-similarity between the acceleration gradient and transformer ratio with respect to the channel size in the linear regime might be attributed to the insufficient channel length, $10\lambda_p$. The plasma oscillation from the small bunch charge density is not strong enough to properly convert the beam energies from deceleration to acceleration. The result implies that a hollow channel thus has a higher gradient than a homogeneously filled plasma column in the blowout regime, and the plasma wakefield acceleration gradient is effectively increased by enlarging the channel size. This result opens the possibility of controlling beam parameters of plasma accelerators for higher gradient and large energy conversion efficiency.

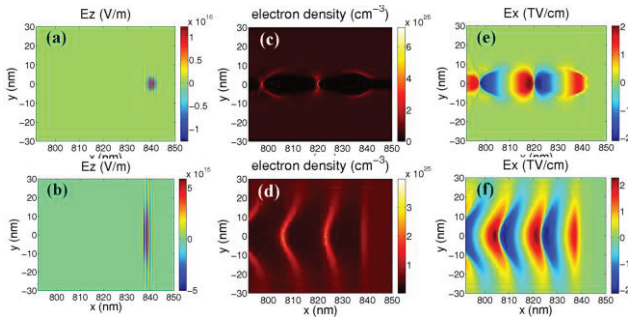

Figure 2: Wakefield excitation with X-ray laser in a tube (top), in comparison with a wakefield in a uniform system (bottom). Distributions of (a)(b) the laser field, (c)(d) electron density, and (e)(f) wakefield in terms of a (a,c,e) tube and (b,d,f) uniform density driven by the X-ray pulse.

The high energy of the photons makes a substantial amount of electrons (either the electrons in the conduction band or in the shallow (< 1 keV) bound electrons) respond to the X-ray fields directly. The high intensity of the X-ray pulse results the instantaneous ionization of some of the bound electrons per atomic site, thereby contributing to free electrons. Even some remaining bound electrons may be treated a solid plasma, where additional optical phonon modes and Buchsbaum resonances are allowed. Two dimensional (2D) particle in cell (PIC) simulations have been performed by using the EPOCH code. The simulation box is 600 nm (x) × 100 nm (y), which corresponds to a moving window with 3000 × 500 cells and 10 particles per cell. For the base case, the laser pulse of wavelength λ_L = 1 nm (corresponding to 1 keV X-ray laser) and normalized peak amplitude of a_0 = 4 means the peak pulse intensity is 2.2×10^{25} W/cm^2. The width in the y-direction and length in the x-direction are $\sigma_L = 5\ \lambda_L$, $\sigma_x = 3\ \lambda_L$, respectively. The tube wall density is given in terms of the critical density by $n_{tube} = 4.55 \times 10^{-3} n_c$. That is, for modeling the nanotube, a solid tube with wall density of $n_{tube} = 5 \times 10^{24}$/cm^3 is used. Tube vacuum radius of σ_{tube} = 2.5 nm is used. The tube location is $2\lambda_L < x < 8000\lambda_L$ and $-50\lambda_L < x < 50\lambda_L$. At t = 0, the laser pulse enters the simulation box from the left boundary.

Fig. 2 shows the comparison between the nanotube case and uniform density case driven by the X-ray pulse. For the uniform density case (Fig. 1(b, d, f)), the Rayleigh length is short due to the small spot size and so the laser pulse quickly diverges as it propagates. Thus the wakefield becomes weaker and disappears due to the defocusing laser field. In this case, the driving pulse

dissipated after propagating a distance of $2000\lambda_L$. However, in the nanotube case (Fig. 2(a, c, e)), the X-ray pulse maintains a small spot size that can be well controlled and guided by the surrounding nanotube walls. The induced wakefield stays stable and the short laser pulse continues propagating even after a distance of $4500\lambda_L$, which is more than twice that of the uniform density case. This stability over a long distance is important for the acceleration to obtain a high energy beam. Considering the real physical parameters, it can be found the wakefield is higher than 2 TV/cm when driven by the X-ray pulse, which is three orders higher than that of the optical laser case (1 eV laser pulse, λ_L = 1 μm, the spot size of σ_L = 5 μm over a length of σ_x = 3 μm, corresponding to 2.2 $\times 10^{19}$ W/cm^2, n_{tube} = 5 $\times$ 10^{18}/cm^3 and tube radius of σ_{tube} = 2.5 μm). This means the energy gain gradient is 2 TeV/cm instead of 2 GeV/cm and opens the possibility to realize a very compact accelerator capable of reaching ultrahigh energies. In addition, the wakefield for the uniform plasma case can be estimated from the $E_0 = a_0^{1\sim2} m_e \omega_p c/e$, which is about $2.2a_0^{1\sim2}$ TV/cm using the parameters in above simulations. This expected value agrees well with the observed one, which means in the narrow limit of the tube, the wakefield scaling resembles that in the uniform plasma formulation.

PLANNED EXPERIMENTS

Two proof-of-concept experiments are currently being planned and prepared at NIU and Fermilab. In the first one, a sample carbon nanotube diffracts the electrons to an image screen, while being pumped by a short-pulse laser. Relativistic electrons are capable of visualizing temporal dynamics of photo-excited lattices in the area of up to a few micrometers with sub-Angstrom of spatial resolution and sub/pico-second temporal resolution. A fraction of the compressed probe beam is diffracted by atomic scatterers in a thin crystal target or a nanostructured substrate. Diffraction peaks will appear on a screen if the diffraction angle is larger than divergence of an un-scattered beam and the coherent and elastic scattering intensity is larger than the background noise. If the probe electrons gain energy from an oscillating plasma wave during the scattering process, it will result in a change of diffraction angle deviated from un-pumped one. In principle, an energy gain increases proportional to an interaction length (crystal-target thickness), whereas the thickness is fairly limited by an attenuation of scattered electrons. The diffraction intensity, influenced by a number of scattering events, is peaked in the range of a mean free path length and then exponentially decays as a crystal gets thicker. Therefore, if the electrons gain a sufficient amount of energy within that distance, the diffraction peak positions will be shifted beyond the screen resolution. In other words, if a shift of peak positions (or angle deviation) is detected while a sample is pumped by a laser, it will be an indirect identification of photo-excitation of crystal plasma wave coupled with electrons. How distinctly the interference patterns emerge in the scattering process relies on the target thickness relative to the mean free path length of elastically scattered coherent electrons.

Figure 3 (a – d) shows the pump-probe experimental setup at NIU. An electron pump probe diffraction system will be employed for this experiment. A laser pulse is split into two paths, one at IR (800 nm) to pump a sample and another tripled to UV (266 nm) to generate a probe (electron) from a photo-cathode in a RF gun. The 150 fs pump laser is coupled with a sample at 30° incidence angle ($\theta_{laser} = \cos^{-1}(\upsilon_e/c)$) that is for velocity matching with an electron probe. The photo-electron beam accelerated up to 0.5 – 1 MeV by the RF-gun is squeezed by a bunch compressor and synchronously injected into the sample with the laser pulse. Currently, the lab is being constructed for an initial beam test (Fig. 3(c) and (d)).

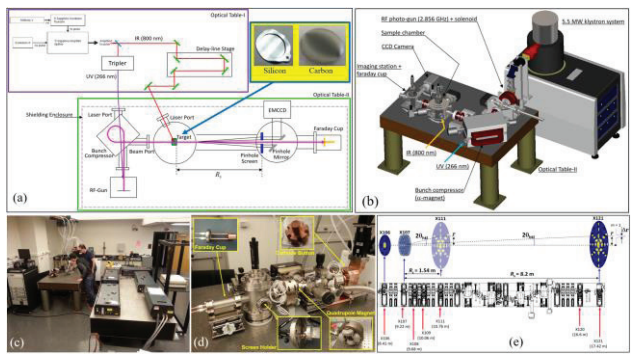

Figure 3: (a) NIU-UED system outline for a low energy (0.5 MeV) (b) 3D-CAD drawing of the designed UED system (c) NIU-UED lab under construction (d) initial beam test setup (e) Experimental setup at FAST facility for a high energy (50 MeV) pump-probe electron diffraction experiment.

Another proposed experiment is also being planned in the 50 MeV electron beamline of Fermilab's FAST facility [10]. Figure 3(e) shows the electron pump-probe experimental setup in the FAST beamline. We will install an extended laser vacuum pipe for the IR pump laser to be injected to a carbon nano-tube target. The FAST 50 MeV linac is designed to operate with nominal beam parameters of σ_r = 0.1 – 1 mm and ε_n = 1 – 5 mm-mrad. There are a few positions to install a target and to image diffractions in the beamline: a sample will be mounted in a frame compatible with the screen holders in an image station in the beamline.

CONCLUSION

Our PIC simulations on beam- and laser-driven channelling acceleration indicate TeV/m scale accelerating gradients in nanotubes. Two demonstration experiments are being planned with a test-lab in NIU and in the FAST facility at Fermilab.

ISBN 978-3-95450-147-2

REFERENCES

[1] T. Tajima, J. M. Dawson, PRL 43(4), 267 (1979).
[2] T. Tajima, PRL 59, 1440 (1987)
[3] P. Chen and R. Noble, SLAC-PUB-4187 (1987).
[4] P. Chen and R. J. Noble, SLAC-PUB-7402 (1998).
[5] V.Shiltsev, Physics-Uspekhy, 182:10, 1033(2012)
[6] Y. M. Shin, APL 105, 114106 (2014)
[7] Y.M. Shin, D. A. Still, and V. Shiltsev, Phys. Plasmas 20, 123106 (2013)
[8] https://www.txcorp.com/vsim
[9] http://www.ccpp.ac.uk/
[10] P. Gabrincius, et al, FERMILAB-TM-2568 (2013)